Size–frequency distributions of fragments from SPH/N-body simulations of asteroid impacts: Comparison with observed asteroid families

Daniel D. Durda [a,*], William F. Bottke Jr. [a], David Nesvorný [a], Brian L. Enke [a], William J. Merline [a], Erik Asphaug [b], Derek C. Richardson [c]

[a] *Southwest Research Institute, 1050 Walnut Street, Suite 400, Boulder, CO 80302, USA*
[b] *Earth Sciences Department, University of California Santa Cruz, Santa Cruz, CA 95064, USA*
[c] *Department of Astronomy, University of Maryland, College Park, MD 20742, USA*

Abstract

We investigate the morphology of size–frequency distributions (SFDs) resulting from impacts into 100-km-diameter parent asteroids, represented by a suite of 161 SPH/N-body simulations conducted to study asteroid satellite formation [Durda, D.D., Bottke, W.F., Enke, B.L., Merline, W.J., Asphaug, E., Richardson, D.C., Leinhardt, Z.M., 2004. Icarus 170, 243–257]. The spherical basalt projectiles range in diameter from 10 to 46 km (in equally spaced mass increments in logarithmic space, covering six discrete sizes), impact speeds range from 2.5 to 7 km/s (generally in 1 km/s increments), and impact angles range from 15° to 75° (nearly head-on to very oblique) in 15° increments. These modeled SFD morphologies match very well the observed SFDs of many known asteroid families. We use these modeled SFDs to scale to targets both larger and smaller than 100 km in order to gain insights into the circumstances of the impacts that formed these families. Some discrepancies occur for families with parent bodies smaller than a few tens of kilometers in diameter (e.g., 832 Karin), however, so due caution should be used in applying our results to such small families. We find that ~20 observed main-belt asteroid families are produced by the catastrophic disruption of $D > 100$ km parent bodies. Using these data as constraints, collisional modeling work [Bottke Jr., W.F., Durda, D.D., Nesvorný, D., Jedicke, R., Morbidelli, A., Vokrouhlický, D., Levison, H.F., 2005b. Icarus 179, 63–94] suggests that the threshold specific energy, Q_D^*, needed to eject 50% of the target body's mass is very close to that predicted by Benz and Asphaug [Benz, W., Asphaug, E., 1999. Icarus 142, 5–20].
© 2006 Elsevier Inc. All rights reserved.

Keywords: Asteroids; Collisional physics; Impact processes

1. Introduction

The known asteroid families are remnants of disruption events that took place millions to billions of years ago within the main belt (e.g., Zappalà et al., 2002). They are identified by their clustered elements in proper semimajor axis, eccentricity, and inclination space (Knežević et al., 2002). By investigating asteroid families, we can glean insights into collisions, the primary geologic processes affecting small bodies in the Solar System, as well as the nature and internal structure of asteroids and planetesimals.

The size–frequency distributions (SFDs) produced by family-forming events are important diagnostic tools in understanding the results of a wide range of fragmentation events. The overall shape of each family's SFD (e.g., average power-law slope index, size of largest remnant vs smaller debris) partially characterizes the nature of the impact that produced it (catastrophic vs cratering, size/speed of impactor, oblique vs head-on). Moreover, detailed features of the SFD (e.g., sizes at which slope changes occur) may yield important clues to the internal structure of the parent body prior to the family-forming event, such as the presence of and/or characteristic size of structural sub-units. The SFD may even carry sufficient information to allow us to compute the original size/mass of the parent body. These insights cannot easily be estimated from the observed fragments for two reasons: (i) an unknown but presumably large

fraction of each family's total mass is in the form of bodies too small to be directly observed using current methods, and (ii) the SFDs of most families have experienced significant modifications over millions to billions of years of collisional evolution. By estimating the size of each family's parent body, we can provide solid constraints for both the unknown disruption law governing asteroid breakups and collisional evolution processes within the main belt over the last several billion years (e.g., Bottke et al., 2005a, 2005b).

Pioneering work in modeling asteroid family SFDs has been done in recent years by Tanga et al. (1999) and Michel et al. (2001, 2002, 2003, 2004a, 2004b). Tanga et al. showed that geometric effects related to the finite volume of fragments from the disruption of a parent body are very important in shaping the resulting SFDs of several observed asteroid families. In particular, they showed, using a relatively simple model that did not rely on a detailed numerical simulation of the fragmentation process, how the overall steepness and morphology of the SFD changes depending on the size of the largest remnant, which in turn is a function of the specific impact energy. That study was the first comprehensive attempt at qualitatively explaining several properties of the SFDs of observed asteroid families. More recently, Michel et al. have carried out impact and reaccumulation simulations using techniques similar to those presented here (namely, coupling a fragmentation code with a particle gravity code). By striking their model parent bodies with projectiles at various impact angles, speeds, and projectile masses, they showed that the size and velocity distributions of select asteroid families are very similar to those produced by the reaccumulation of debris following catastrophic impacts. They also found that satellites form readily as a byproduct of the reaccumulation process. Michel et al. consider both competent and pre-shattered target configurations, most recently focusing on detailed simulations of the Karin cluster (Michel et al., 2003) and the Koronis and Eunomia families (Michel et al., 2004a). Those studies concluded that pre-shattered targets tend to produce collision outcomes in better agreement with those of the real families than do simulations with monolithic parent bodies.

Nesvorný et al. (2006) used similar codes and a revised Karin cluster membership to show that the disruption of an unfractured (monolithic) parent body produces the most satisfactory match to the observed Karin cluster SFD. With the revised Karin cluster membership, Michel et al.'s (2003) simulations with monolithic parent bodies also produce very good matches to the observed SFD.

Motivated by these studies and with new family membership classifications in hand, we investigate in this paper the morphology of SFDs resulting from a wide range of impacts into 100-km-diameter, solid basalt parent asteroids. Our runs are represented by a suite of 161 SPH/N-body simulations conducted to study asteroid satellite formation (Durda et al., 2004). We scale and compare these modeled SFDs with those of the observed main-belt asteroid families (thus effectively scaling the 100-km-diameter target to target sizes applicable to the observed families) in order to shed light on the circumstances of family formation and the size of the parent asteroid. We believe

the matrix of runs described here, once scaled, cover most of the impact scenarios that take place in the main belt. Our model and results are presented below.

2. Numerical technique

The results presented here are derived from the same suite of impact simulations presented in Durda et al. (2004); we summarize only briefly here the numerical techniques used in the simulations and refer the reader to Durda et al. (2004) for further details. Recent reviews of asteroid collisional disruption, including observations, experimental scaling, and computational modeling, are found in Ryan (2000), Holsapple et al. (2002), and Asphaug et al. (2002).

We model the collision phase of cratering and catastrophic impacts between two asteroids with the 3-dimensional SPH code SPH3D (Benz and Asphaug, 1995), which models shock propagation in elastic solids, utilizing the von Mises plastic yield criterion for intense deformation together with an explicit fracture and dynamic fragmentation model acting on the principal tensile component of the stress tensor during brittle deformation. Gravitational self-compression of the target during the impact phase is treated as an overburden stress that must be exceeded before fracture can initiate (Asphaug and Melosh, 1993). We utilize a Tillotson equation of state model (Tillotson, 1962) for basalt. In our satellite formation work with these simulations, we found that the modeled collision outcomes for targets with 100,000 or more particles matched each other sufficiently well that we concluded that we achieved resolution convergence for fragments a few to several kilometers in diameter.

Once the impact phase of the simulations is complete (ejecta flow fields established with no further fragmentation/damage), the outcomes of the SPH models are handed off as the initial conditions for N-body gravitational simulations using the code pkdgrav (Richardson et al., 2000; Leinhardt and Richardson, 2002; Leinhardt et al., 2000; Stadel, 2001). pkdgrav is a scalable, parallel tree code for modeling the gravitational interactions between the resulting fragments, with the ability to rapidly detect and accurately treat low-speed collisions between particles, thus allowing for realistic modeling of the formation of rubble pile accumulations among ejected fragments. Low-speed collisions between debris fragments are treated as mergers resulting in a new spherical particle of appropriate combined mass and equivalent diameter.

The N-body phase of each simulation is run to about 4 days after the impact. As described in Durda et al. (2004), our choice of 4 days of N-body simulation time after impact was set by a combination of available CPU resources and limitations inherent in the simulations due to the fact that irregular primary asteroid shapes are not preserved and mutual tidal interactions are not included. We note that for some of the more highly catastrophic impacts, where a great deal of small debris is ejected at high speed, 4 days may not provide sufficient time for the gravitational reaccumulation phase to run its full course. For instance, some of the Koronis family simulations performed by Michel et al. (2003), in which the largest remnant

mass was only ~4% of the parent body mass, required up to 11 days of simulation time because some significant reaccumulations were still taking place. We have performed a number of 'spot checks,' running nearly two dozen of the N-body simulations to approximately 16 days after the impact, in order to sample the degree of convergence in our 4-day N-body simulations. In general, we do indeed see the greatest differences in final largest remnant diameter among the most energetic of our simulated impact events, but even in these cases we find that the largest remnant diameters increased by at most only a few percent, with a negligible change in the morphology of the family SFD. Still, we urge caution when interpreting the results of our most catastrophic impact simulations.

The target asteroids in this study are 100-km-diameter solid basalt spheres. The spherical basalt projectiles range in diameter from 10 to 46 km (in equally spaced mass increments in logarithmic space, covering six discrete sizes: 10, 14, 18, 25, 34, and 46 km), impact speeds range from 2.5 to 7 km/s (generally in 1 km/s increments, bounding the range of typical mutual impact speeds in the main belt (Bottke et al., 1994)), and impact angles range from 15° to 75° (i.e., nearly head-on to very oblique) in 15° increments. Details of each of the simulation outcomes are presented in Table 1 of Durda et al. (2004).

3. Results

3.1. Largest remnant mass ratio vs specific impact energy

The large number of simulations completed for this study allows comparison with results of previous laboratory impact experiments giving the largest remnant to target mass ratio (M_{lr}/M_{targ}) as a function of the specific impact energy (KE_{imp}/M_{targ}). Fujiwara et al. (1989) present a compilation of such data for various material types and experimental conditions in their Fig. 2. The prevalent feature of the $\log(M_{lr}/M_{targ})$ vs $\log(KE_{imp}/M_{targ})$ plot in that figure is the linear trend of the data, with a slope index of about -0.79. We have reproduced this plot for our matrix of SPH/N-body simulations (Fig. 1), separating the results by impact angle. We see a similar linear trend in our results in the regime of catastrophic fragmentation, but with significantly steeper slopes (approximately -2.6 for impact angles of 15° and 30° and about -3.7 for an impact angle of 45°) and a possible upturn deviating from the linear trend for the most catastrophic impacts. The gentle rollover toward $M_{lr}/M_{targ} = 1$ for the low-energy, cratering impacts is not observed in the laboratory experiments. The steepening of the linear portion of the plot for our simulation results may be a product of the substantial gravitational reaccumulation that occurs among the impact debris in these simulations. At modest impact energies in the catastrophic disruption regime the largest remnants can grow significantly more massive over time than their initial masses immediately after the impact, moving their data points upward on the plot relative to data points for more energetic impacts where less reaccumulation takes place. No such gravitational reaccumulation can occur in the laboratory-scale experiments.

3.2. SFD morphologies

Before describing our model results in more detail, we introduce here nomenclature that we use to describe some attributes of SFD morphologies and to refer to particular model runs. The overall shape of the SFD tends to be more 'concave' (i.e., steep slope at small member sizes but shallow slope at large member sizes, so that relatively more members are small) for the lowest-energy events (cratering events, produced by impacts by small and/or low-speed projectiles) and more 'convex' (i.e., shallow slope at small sizes but steep at large sizes, so that relatively more members are large) for the higher-energy events (supercatastrophic disruption, produced by impacts with large and/or high-speed projectiles). More explicitly, a barely catastrophic disruption event is defined as one where 50% of the target is ejected at escape velocities. Cratering events are then defined as those where much less than 50% of the ejecta escapes, while supercatastrophic disruption events are those where much more than 50% escapes.

Fig. 2 illustrates our use of the terms 'convex' and 'concave' in the context of this study. We name the output of a particular impact simulation with respect to the target material, the impact speed, the impact angle, and the logarithm of the target-to-projectile mass ratio, respectively. Thus, for example, model Basalt_5_30_1.8 involved a 100-km-diameter solid basalt target, impacted at 5 km/s at a 30° impact angle by a 25-km-diameter projectile.

The fragment SFDs resulting from the suite of 161 SPH/N-body simulations display a wide range of morphologies, as displayed in Fig. 3. Most generally, and as intuition would lead one to expect, for a given impact speed low-energy impacts result in cratering events while high-energy impacts result in catastrophic to super-catastrophic events. Low impact energies can be achieved by small impactor size and/or low impact speed and/or a large impact angle.

At a given impact angle, the lowest-energy impacts produce SFDs with a single very large remnant and a somewhat concave SFD for fragments smaller than ~5 km. At the highest impact speeds we have run (7 km/s) the second-largest fragments have diameters of about 7 or 8 km so that the SFD for the cratering debris becomes very much more concave.

At a given impact speed, the size of the largest remnant decreases with increasing impactor size while the size of the second-largest fragment increases, so that concave cratering SFDs begin to transform into more linear, power-law-like SFDs. At the transition between these two SFD morphological regimes the largest remnant has a diameter of ~20 km, corresponding to a largest remnant-to-original target mass ratio, M_{lr}/M_{targ}, of ~0.008. That transition occurs at smaller impactor sizes for greater impactor speeds and at greater impactor sizes for larger impactor angles. This perhaps rather obvious behavior follows the results of Tanga et al. (1999) who showed quite effectively, with a purely geometric model of the disruption process, that what really drives the change in overall SFD morphology is the size of the resulting largest remnant.

Impacts that maximize the number of similar-size largest remnants (at ~20 km, $M_{lr}/M_{targ} \approx 0.008$) occur at impact
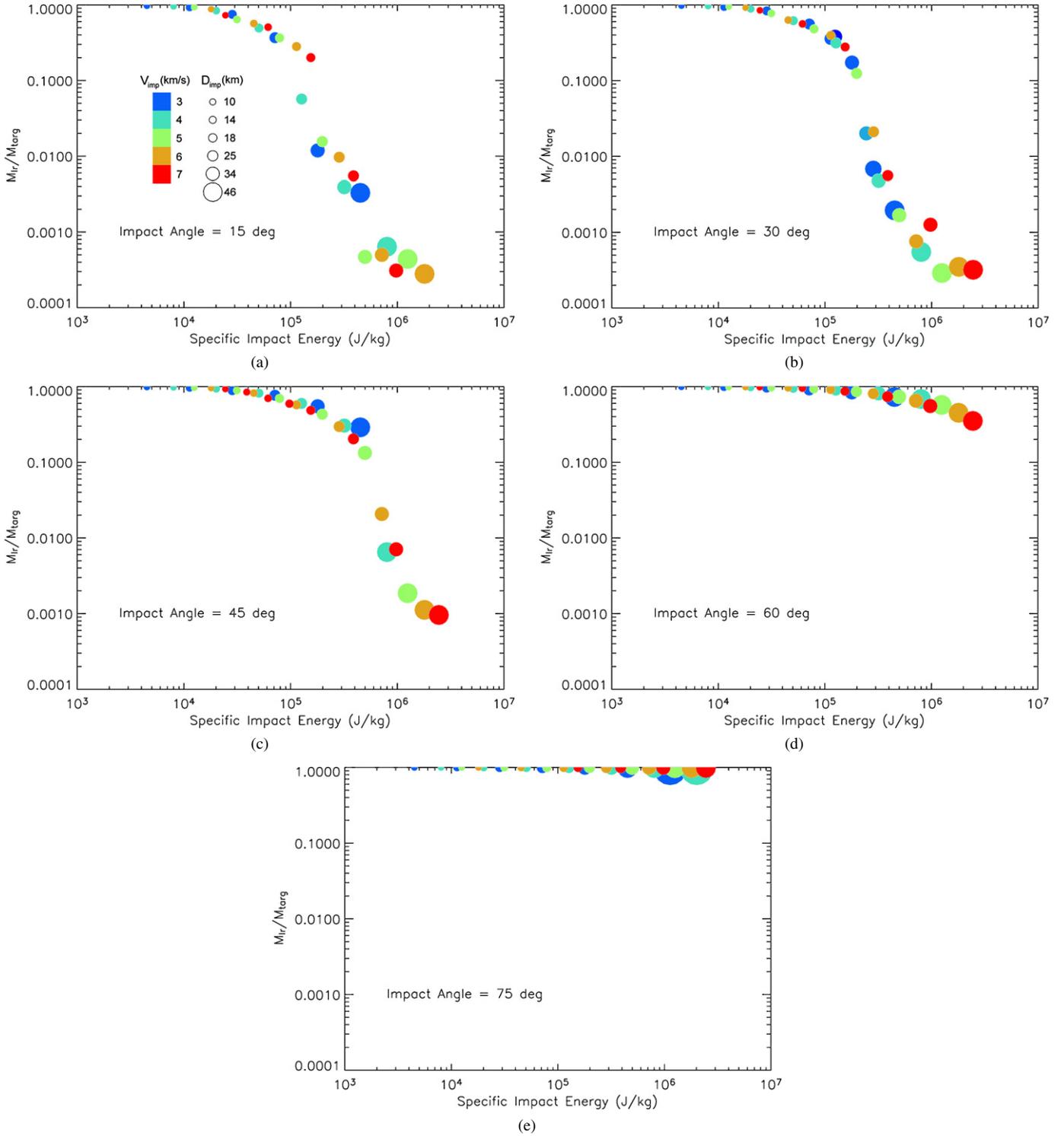
Fig. 1. Largest remnant mass ratio versus specific impact energy for our SPH/*N*-body simulation results, for an impact angle of 15° (a), 30° (b), 45° (c), 60° (d), 75° (e). The inset shows the color and size coding for the data points, keyed to impactor speed and diameter.

speeds of 4–6 km/s with 25–34-km-diameter impactors, requiring larger impactors at higher speeds for more oblique impacts and smaller impactors at lower speeds for more head-on impacts. These same impacts also produce SFDs with the shallowest slopes overall. There seems to be a greater tendency for the SFD to become somewhat 'humpy' (i.e., to display a significant convex hump for the largest fragments) near this impact

regime for more head-on impacts than for more oblique ones. Knowledge of other details of the collision outcome, such as the shape of the fragment ejection velocity field, are required in order to fully characterize the impact angle for any particular family, however.

The transition point where 'concave' cratering SFDs begin to transform into more linear power law SFDs occurs at smaller
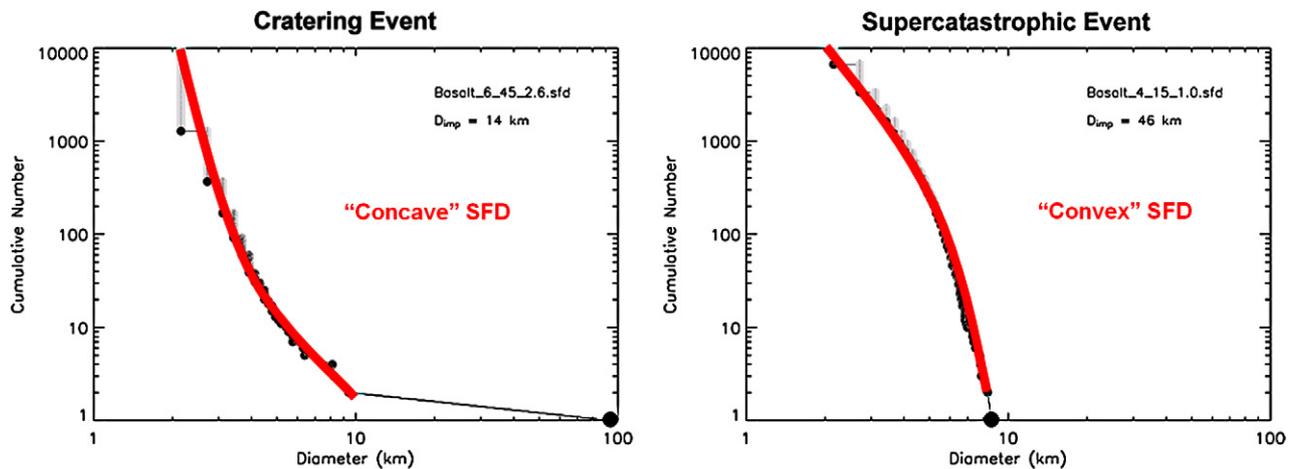
Fig. 2. 'Concave' versus 'convex' SFDs.

impactor sizes for greater impactor speeds and at greater impactor sizes for larger impactor angles. Impacts that maximize the number of similar-size largest remnants (at ~20 km) occur at impact speeds of 6–7 km/s with 25–34-km-diameter impactors; larger impactors at higher speeds are required to achieve the same results for oblique impacts as for smaller impactors at lower speeds impacting more nearly head-on. The SFDs with the very shallowest slopes overall derive from impacts at about 4–6 km/s with 25–34-km-diameter impactors.

Examination of Figs. 3a–3c reveals a broad boundary separating cratering impacts from supercatastrophic disruption. This threshold catastrophic disruption 'corridor' represents the varying combination of impactor size and speed that carries the same Q_D^* threshold specific energy necessary for catastrophic disruption (i.e., impacts that leave a largest remnant with 50% the mass of the original target asteroid). Impacts to the upper left above the corridor are cratering collisions, while impacts to the lower right below the corridor are supercatastrophic disruptions. There is some hint that the morphology of the SFD changes from more convex to more concave as one moves along the corridor to the upper right—to smaller, faster impactors. We speculate that perhaps the larger, slower impactor combination allows for more gravitational reaccumulation among the larger debris, contributing to the convexity of the SFD, than does the higher energy density of the smaller, faster impactor combination, which creates more of a 'spray' of cratering-type debris. The catastrophic disruption corridor shifts to the lower right (to higher energy through larger, faster impactors) from Figs. 3a–3c as impacts become more and more oblique. The corridor all but disappears off the bottom right of Fig. 3d and is not present at all in Fig. 3e; the oblique 60° and 75° impacts in these simulations result almost entirely in cratering collisions.

3.3. Comparison of modeled SFDs with observed asteroid families

A visual inspection of the complete suite of simulation results shows that these modeled SFD morphologies match very well the variety of observed SFDs of actual asteroid families (Fig. 4). The families were determined using clustering algorithms that look for similar proper semimajor axis, eccentricity, and inclination values (Zappalà et al., 2002). Our formal procedure for determining families is described in Nesvorný et al. (2003). The diameters of the family members were computed from their absolute magnitudes and albedos. Where possible, we used the albedo of the objects cited in the literature. In most cases, however, this information was unavailable. To circumvent this problem, we assumed that small objects in a family had the same albedo as the larger members of the family and/or albedos representative of the same taxonomic class (Cellino et al., 2002).

Some main-belt families are known or suspected to have interlopers among their larger members based on spectroscopic observations as a proxy for plausible mineralogical composition (e.g., Cellino et al., 2002; Table 1). Since the presence of these interlopers can affect the morphology of the observed family SFDs, the individual interlopers have been removed from the family SFDs before comparison with our modeled SFDs. Those families are indicated with "noint" appended to the family name in Fig. 4 and the SFD plotted is the family SFD 'cleaned' of known or suspected interlopers. See Table 1 for details of which asteroids were removed in these cases. In at least one case, the (410) Chloris family, the inability to match the observed SFD with anything from our matrix of simulations hints at the presence of otherwise unidentified interlopers; our models suggest that either the largest or second largest member of that family is an interloper.

Our modeled SFDs can be used to estimate the parent body diameter (D_{PB}) of observed asteroid families by plotting the (morphologically matching) modeled SFD and the observed family SFD to the same scale on the same plot. This assumes, of course, that collision outcomes are scalable to the observed families. While this approximation appears to be reasonable (to zeroth order) for most observed families, we caution that it may well break down when the gravitational acceleration of the family's parent body is significantly larger or smaller than our model parent body. Recalling that the modeled family assumed a 100-km-diameter parent body, the resulting largest remnant and SFD of associated smaller fragments may need to be offset to the left or right to match the observed SFD, suggesting a
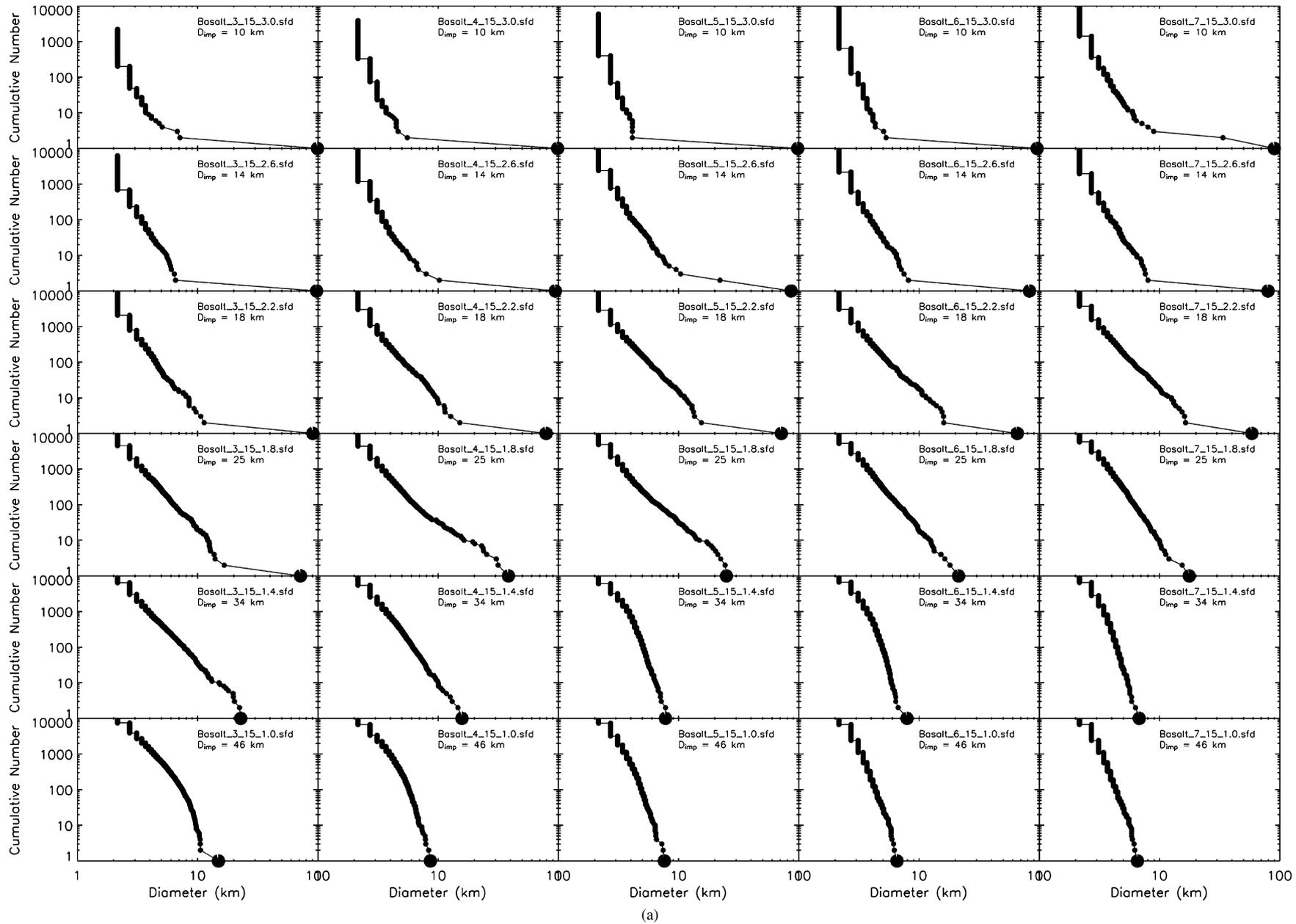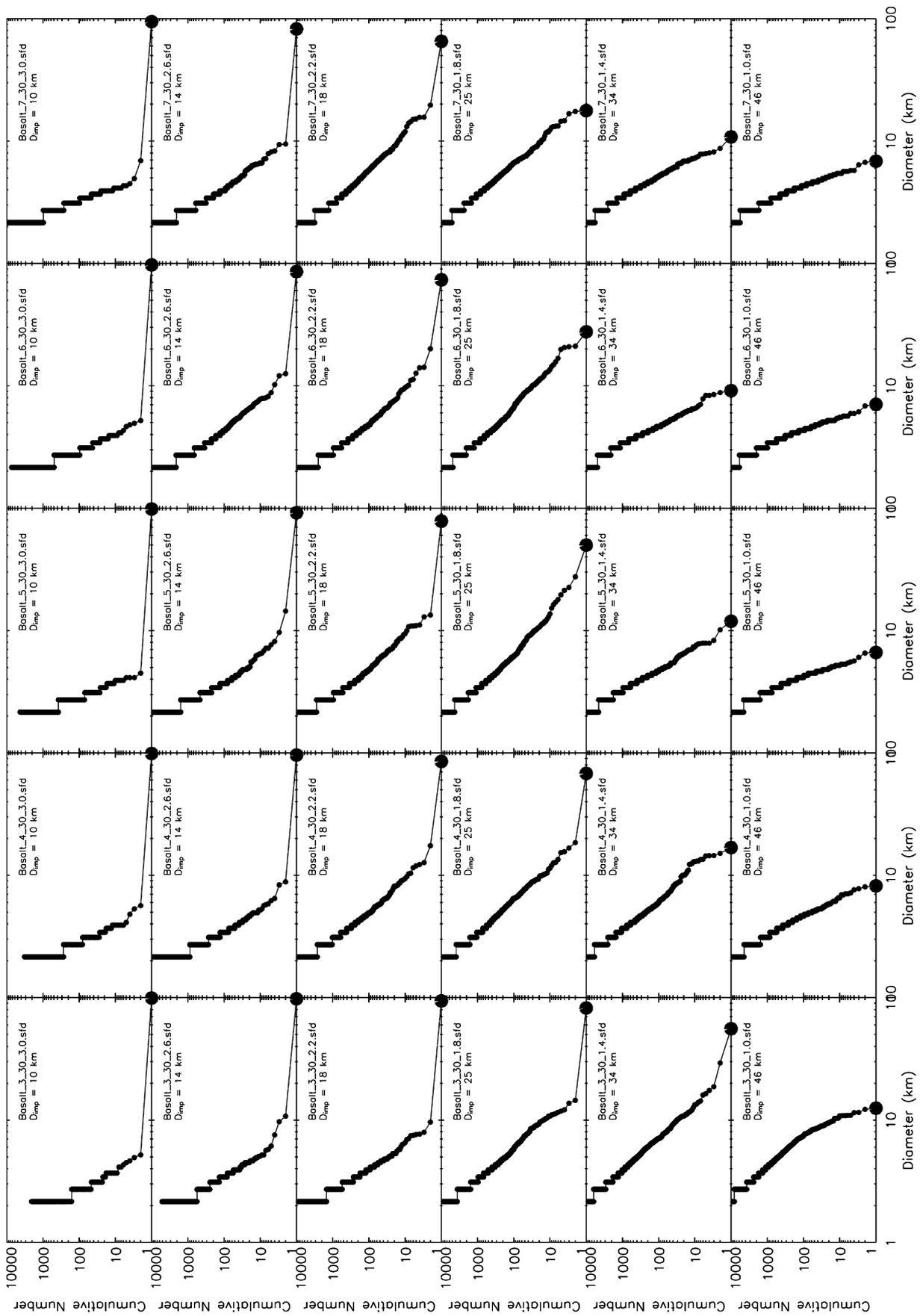
Fig. 3. Modeled SFDs for an impact angle of 15° (a), 30° (b), 45° (c), 60° (d), 75° (e). Impact circumstances are arranged with impact speed increasing from left to right, and impactor size increasing from top to bottom. The large black dots highlight the size of the largest remnant.
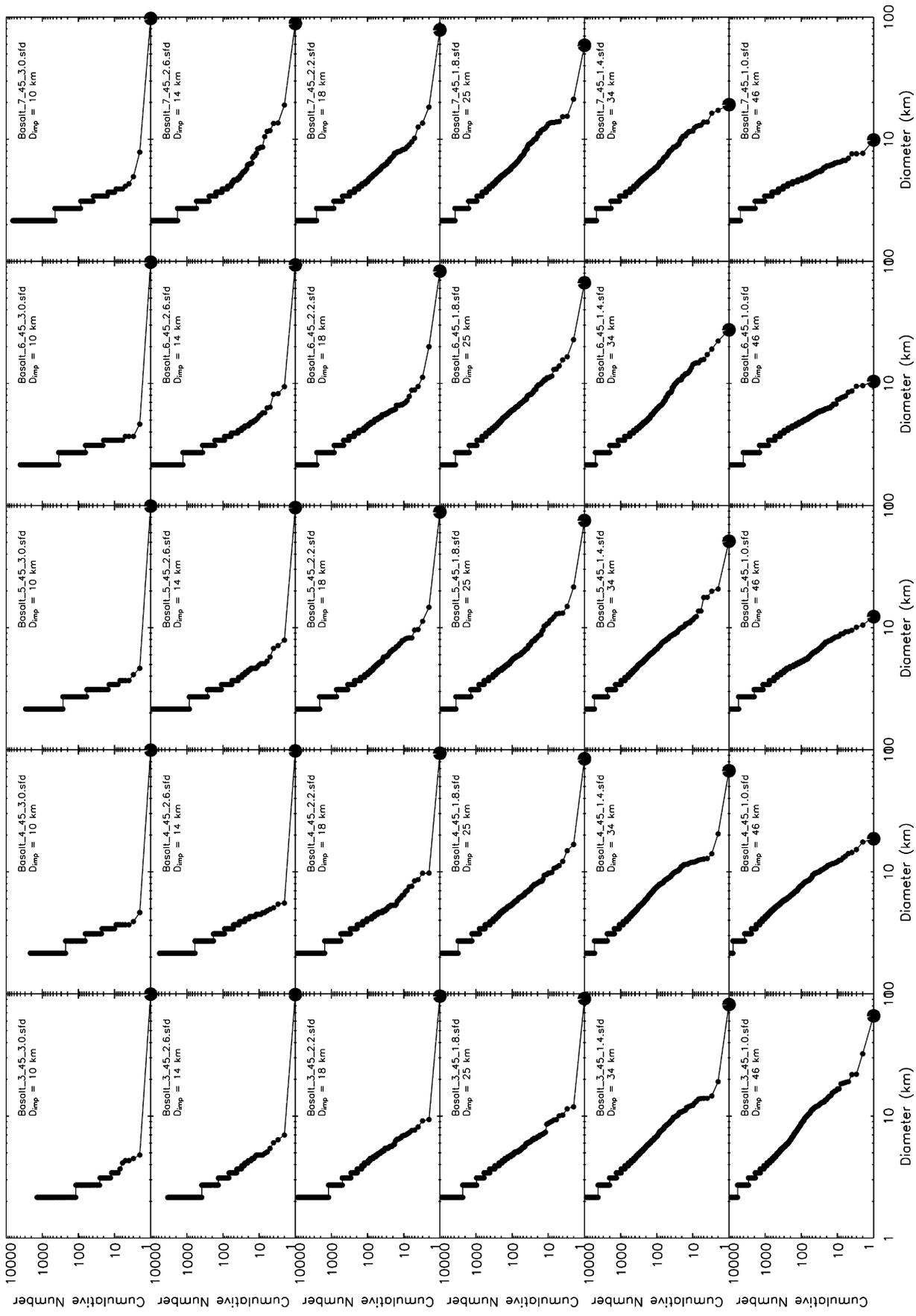
Fig. 3. (*continued*)
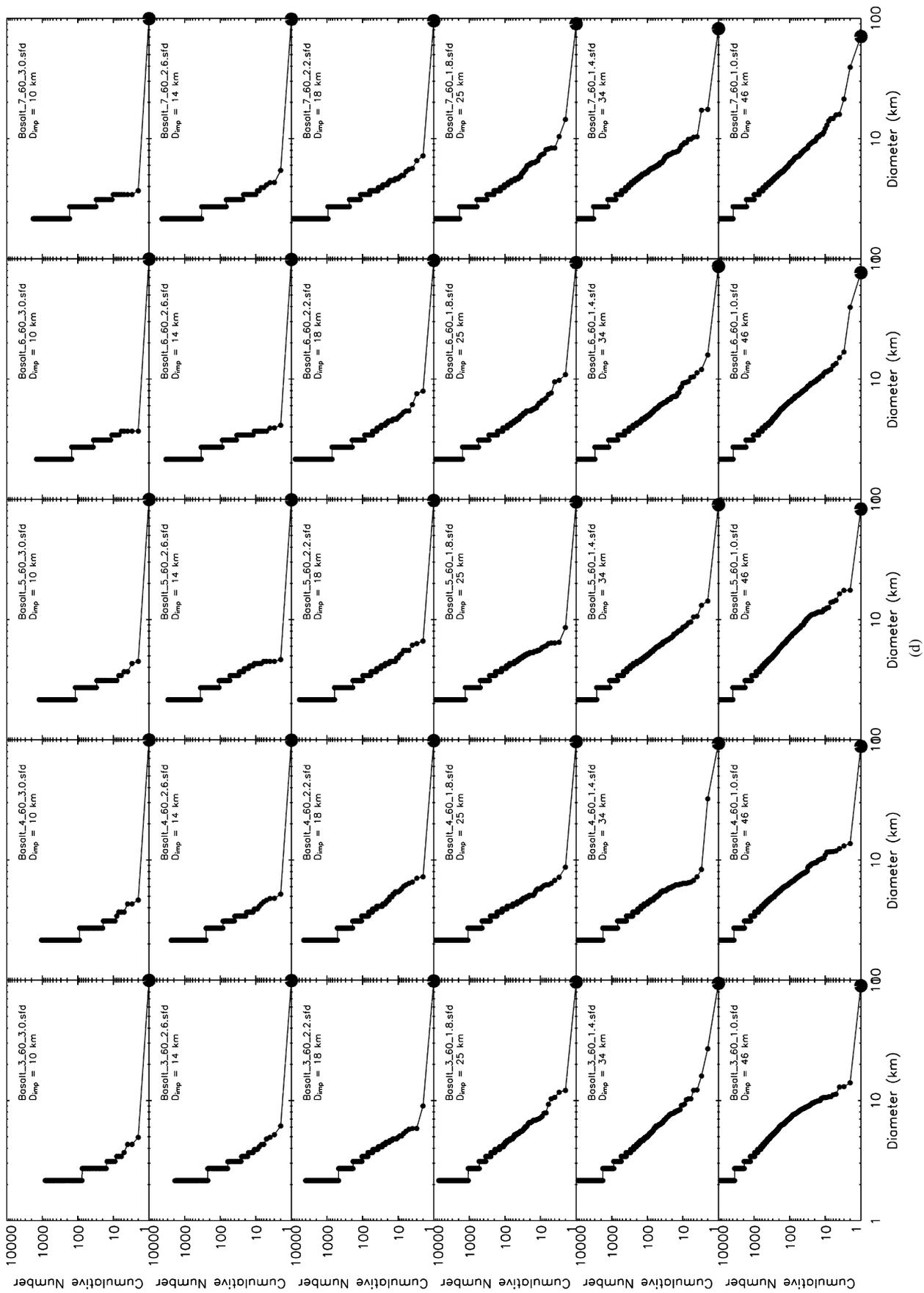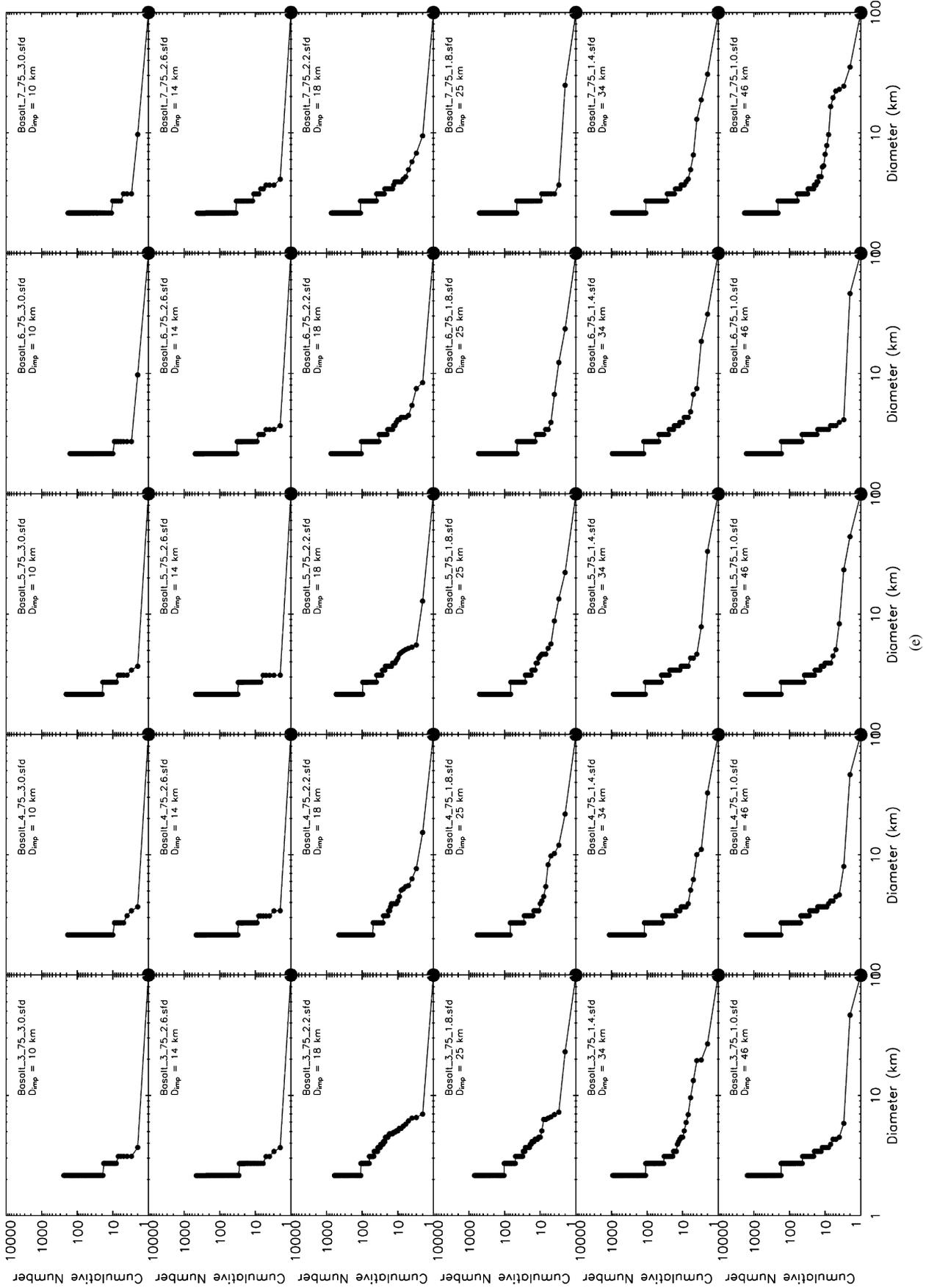
Fig. 3. (*continued*)
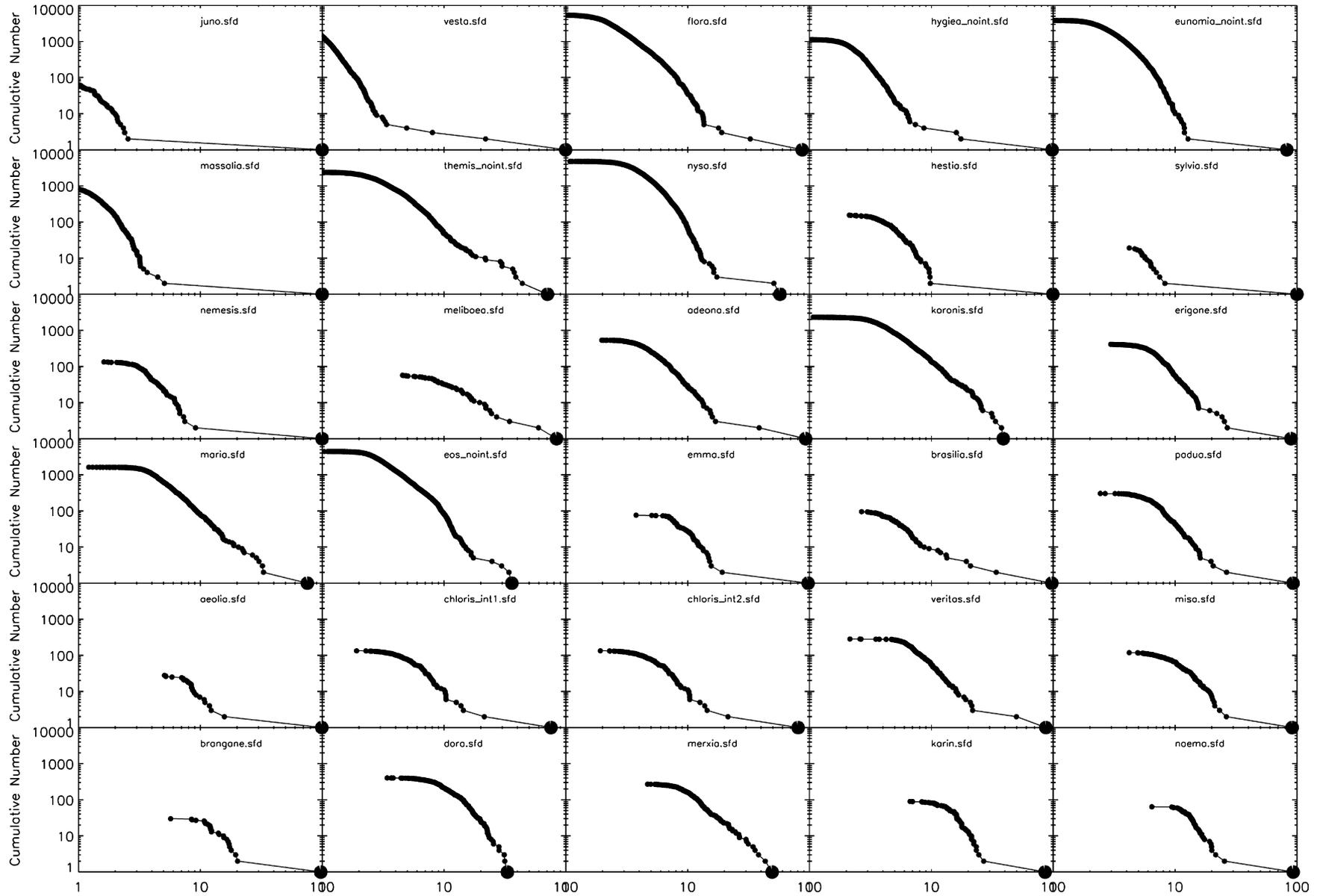
Fig. 3. (*continued*)

Fig. 3. (*continued*)

Fig. 4. Observed SFDs of main-belt asteroid families (Nesvorný et al., 2005), plotted to the same scale as the modeled SFDs in Fig. 3. For those families with known or suspected interlopers, the SFD is presented with the interlopers removed and the family name is appended with the label "noint." See Table 1 for notes.
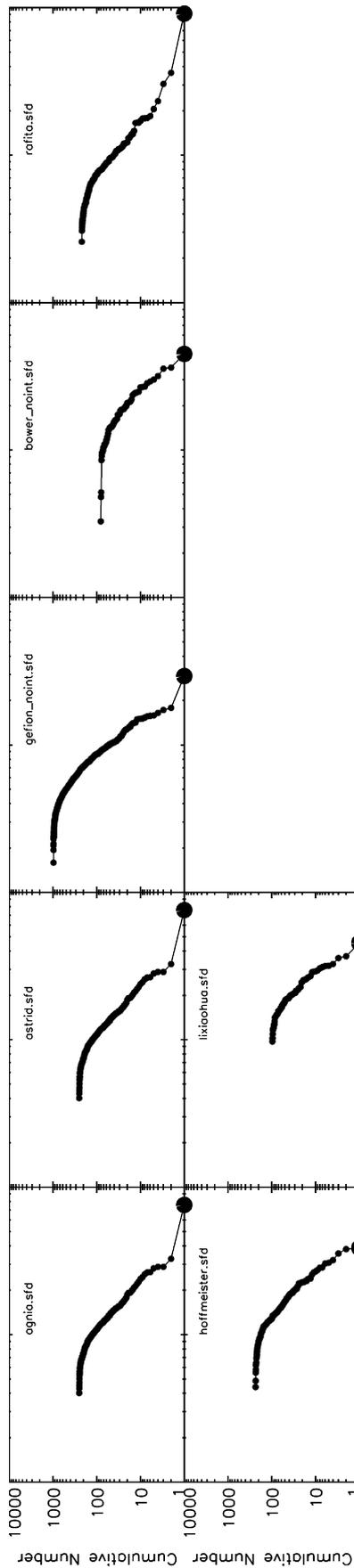
Fig. 4. (*continued*)

larger or smaller parent body for the observed family, respectively. The magnitude of this offset in logarithmic units yields the factor increase or decrease in the diameter of the actual family parent body from the 100-km-diameter parent body of the modeled family. Hence, this method of deriving the actual family parent body diameter by scaling from our 100-km parent body simulation results assumes that the impact outcomes scale linearly with parent body size. See Section 4 for further discussion.

We have developed an objective, numerical algorithm for performing these fits that is least-squares-like in operation. The algorithm is a particle cloud overlap method that simply minimizes the sum of the distances between each pair of observed and modeled SFD points as the modeled SFD is 'slid' horizontally past the observed family SFD in $\log(N)$ versus $\log(D)$ space, where N is the cumulative number of objects with diameter larger than D. The pair distances are weighted by the inverse square of the root N error assumed for each point in the cumulative SFDs. The observed and modeled SFDs are 'truncated' prior to the fitting routine: we do not include observed family members below the apparent observational completeness limit (these would, of course, bias the fit), and we limit the number of fragments in the modeled family to the same number as above the completeness limit of the observed family. Tests of this fitting algorithm demonstrate that the numerical fits agree very nicely with those previously obtained 'by eye' (i.e., Durda et al., 2003), and they have the benefit of being more objective than the simple 'eyeball' method (i.e., Bottke et al., 2005a), with more formal estimates of the error in the fits.

We illustrate this fitting technique for the case of the (1726) Hoffmeister family (Fig. 5). Visual comparison of the features of this family's SFD (size of largest remnant, largest remnant size to second-largest remnant size ratio, overall shape and slope index, etc.) with those of similar modeled SFDs yields rough agreement with several models in our suite of simulations and best agreement with one in particular—Basalt_7_45_1.4 (a supercatastrophic disruption resulting in a ~20-km-diameter largest remnant). Shifting the modeled SFD to the right by a factor of ~1.5 results in a very good match to the observed (1726) Hoffmeister family SFD, suggesting that this family resulted from the supercatastrophic breakup of a ~150-km-diameter parent object. Note that this parent body size is considerably larger than the ~69-km-diameter parent body size derived by merely summing the volume represented by the observed family members. Significant discovery incompleteness at diameters smaller than about 9 km misses much of the mass in this family, suggesting that ~90% of the mass of this family is unaccounted for observationally. If this result is generally applicable to other families as well, then there is considerable "missing mass" in the main asteroid belt, at least from the point of view of the production of small family members (Zappalà and Cellino, 1996). The derived shape of the main-belt SFD by Bottke et al. (2005a, 2005b), however, is shallow; this implies that family SFDs experience sufficient collisional evolution after formation. According to modeling results, these steep SFDs eventually erode back to the same shape of the background main-belt SFD (Bottke et al., 2005c). This may explain why so
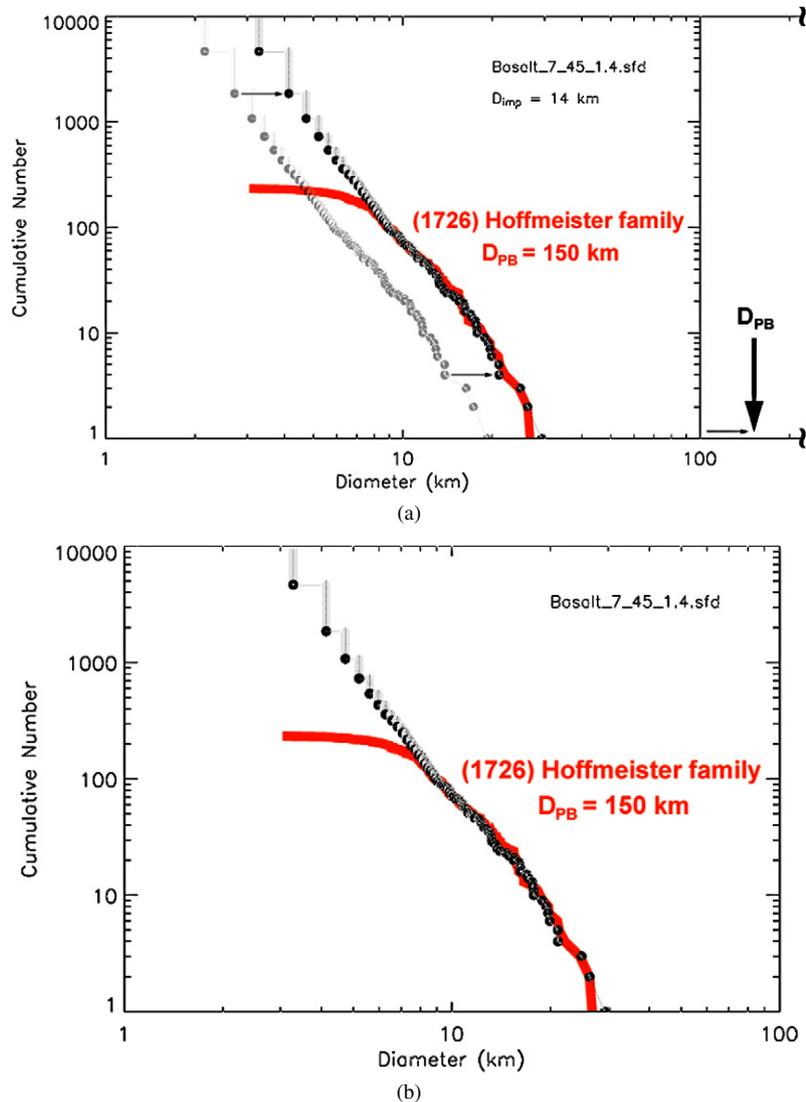
Fig. 5. An illustration of the numerical routine for fitting a modeled SFD to an observed main-belt asteroid family, in this case the (1762) Hoffmeister family. (a) The candidate modeled SFD, plotted in gray, must be shifted to the right by a factor of 1.5 in order to fit the observed SFD. This suggests a parent asteroid a factor of 1.5 larger than the 100-km-diameter target asteroid assumed in the simulation. (b) Best fit of the Basalt_7_45_1.4 model SFD to the observed (1726) Hoffmeister family SFD.

many families have shallow slopes for $D < 5$ km (Morbidelli et al., 2003).

The results of our fitting routine depend on subjective decisions that must be made as to where lies the observational completeness limit in the observed family SFD (which we take to be the size at which the roughly power-law-like trend starts to become significantly shallower) and where the modeled SFDs should be truncated when performing the fit. We examined the dependence of our results on these decisions by varying these cutoff limits. With the observationally complete (1726) Hoffmeister family limited to 100 members, we truncated the Basalt_7_45_1.4 modeled SFD to 200, 100, and 43 members and ran our fitting routine. The resulting offset factors were 1.524, 1.503, and 1.435, respectively. When the number of members in the observed family SFD was changed to 200 and the modeled family truncated to 400, 200, and 100 members, the resulting offset factors were 1.528, 1.500, and 1.455,

respectively. These results suggest that the uncertainty in the derived parent body diameter resulting from the fitting routine itself is only of order a few kilometers; for this model fit we derive a parent body diameter of 150 km, with an uncertainty of about 3–4% depending on the choice of completeness cutoff. This 'internal' fit error is significantly less than the difference in derived parent body diameter obtained with the other candidate model SFD (i.e., 118 km, from the simulation Basalt_3_15_1.4; see Table 1) and less than the uncertainties inherent in the technique itself, as discussed in Section 4 below.

We illustrate another example, this time with a family for which the observed SFD suggests a cratering impact rather than a catastrophic disruption. Visual comparison of the features of the (283) Emma family's SFD with our model results suggests a good match to the simulation Basalt_4_15_2.2 (Fig. 6). As for the (1726) Hoffmeister family above, we ran several fits with various choices of SFD cutoffs. With the observation-
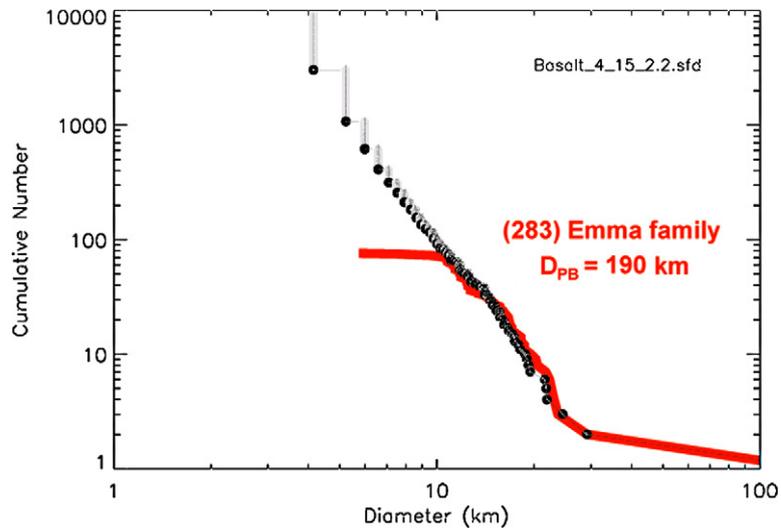
Fig. 6. Same as Fig. 5b, but for the (283) Emma family. The largest member of this family, (283) Emma itself, lies just off the right edge of the plot at a diameter of 148 km.

ally complete family limited to 68 members and the modeled SFD truncated to 136, 68, and 34 members, the resulting offset factors were 1.935, 1.905, and 1.876, respectively. With the observationally complete family limited to 34 members and the modeled SFD truncated to 68, 34, and 17 members, the resulting offset factors were 1.949, 1.914, and 1.880, respectively. Again, the internal error due to the fitting routine itself is only of order a few percent; for this model fit we derive a parent body diameter of 190 km. The model Basalt_3_30_1.8 is also a good match to the observed morphology of this family, yielding a parent body size estimate of 180 km.

The results of our analysis for the families examined by Nesvorný et al. (2005) are presented in Table 1. A few families from the Nesvorný et al. (2005) study (e.g., 4652 Iannini and 18405 FY12) were not examined here due to the very small number of members in those families and the likelihood of significant discovery incompleteness even among the largest family members. The model fits in Table 1 are listed in descending order of 'goodness' of fit within each family, as measured by the normalized sum of the distances between the observed and modeled SFDs. Because the fitting routine weights more highly the larger number of smaller fragments, there are several cases where a more subjective visual inspection of the fit reveals that features of the SFD among the larger, less numerous fragments would seem to be more important in assigning a good fit; in these cases we have manually ordered the fits accordingly.

4. Discussion

4.1. Caveats in our modeling results

As discussed above, there are uncertainties in the derived parent body diameters associated with the numerical fitting algorithm we have adopted. There are other, probably larger and more difficult to quantify, uncertainties inherent in our fitting technique that result from (1) trying to scale the results of simulated impacts into 100-km-scale targets to significantly larger or

smaller parent bodies, and (2) the fact that we attempt to match observed family SFDs to a coarsely sampled matrix of impact simulations originally run for a purpose other than for matching SFD morphologies. One might expect that the results of actual simulations involving significantly larger or smaller parent bodies might vary from the scaled results presented here because of enhanced or decreased gravitational effects among the debris in larger- or smaller-scale impacts. Also, close inspection of Fig. 3 reveals some rather significant changes in SFD morphology when crossing some impactor size and/or impactor speed boundaries; if one were trying to find a morphological match for a particular observed SFD in such a region, the closest available match might not necessarily be the best that could be achieved if the phase space matrix was sampled more finely.

For example, our best fit for the diameter of the (832) Karin cluster parent body is 63 km, derived by less-than-optimal morphological matches by three simulations: Basalt_7_15_2.2, Basalt_7_30_2.2, and Basalt_7_45_1.8. On the other hand, Nesvorný et al. (2006) conducted over 100 detailed SPH/N-body simulations for the formation of this family alone, and derived a parent body diameter of 31 ± 3 km. The simulation Basalt_7_15_2.2 does a fair job at fitting the 'power law' of small debris from the second largest fragment down to smaller fragments, but the largest remnant is just a bit larger than that actually observed for the Karin cluster. In other words, the difference in size between the largest remnant and the second largest fragment produced in this simulation is just a bit larger than for the real Karin cluster. The fitting algorithm, which weighs more heavily the morphological fit for the small debris, forces the largest remnant to be too large, and this drives up the overall size of the reconstructed parent body—to 65 km diameter in this case. The simulation Basalt_7_30_2.2 produces a better match to the difference in size between the largest remnant and the second largest fragment, but then the 'power law' of smaller debris is offset too far to smaller sizes if we manually fit the observed SFD by considering the largest and second largest fragments as the most important feature of the morpho-

Table 1

Comparison of observed and modeled main-belt asteroid families

Family	Simulation	Shift factor[a]	Mean D_{PB} (km)	Spectral characteristics[b]	Notes
3 Juno				S type	Cratering impact outside the regime covered by our models (none of our models produce a secondary-to-primary size ratio as low as 0.0255).
4 Vesta	Basalt_6_75_1.8	4.12	425	V type	Cratering regime, best fit by large, high-speed impactors at very oblique angle.
	Basalt_7_75_1.8	4.38			
8 Flora	Basalt_6_45_1.8	2.01	185	S/C type	Concave nature of SFD near 10 km size suggestive of large impactor at oblique angle.
	Basalt_3_45_1.4	1.73			
	Basalt_6_60_1.0	1.81			
10 Hygiea	Basalt_7_15_3.0	4.42	442	C (10 Hygiea) and B type	Interlopers. Asteroids 100, 108, 1109, 1209, and 1599 (object number 2, 3, 6, 7, and 8) removed from the SFD for the fit. Morphologically very similar to Basalt_3_30_2.6 or Basalt_3_60_1.8, but with a [larger] D_{LR}/D_{SLR} ratio.
15 Eunomia	Basalt_4_60_1.0	2.96	292	S type	Interlopers. Asteroids 85 and 141 (object number 2 and 3) removed from the SFD for the fit.
	Basalt_3_60_1.0	2.88			
20 Massalia	Basalt_5_60_3.0	1.43	144	S type	
	Basalt_4_60_3.0	1.44			
	Basalt_3_60_3.0	1.46			
24 Themis	Basalt_5_30_1.8	4.51	451	C type	Interlopers. Asteroids 461 and 1171 (object number 9 and 23) removed from the SFD for the fit.
46 Hestia	Basalt_7_15_2.6	1.56	153	S type	
	Basalt_6_15_2.6	1.51			
87 Sylvia	Basalt_4_60_1.8	2.70	272		
	Basalt_5_45_2.6	2.73			
	Basalt_6_60_2.2	2.72			
128 Nemesis	Basalt_5_60_1.8	1.98	197	C type	
	Basalt_4_60_1.8	1.95			
137 Meliboea	Basalt_7_60_1.0	2.48	248	C type	Big, fast impactor at very oblique angle.
145 Adeona	Basalt_6_60_1.0	1.87	185	C type	Also reminiscent of Basalt_3_45_1.4 ($D_{PB} = 180$ km) and Basalt_4_45_1.4 ($D_{PB} = 183$ km).
	Basalt_7_60_1.0	1.84			
158 Koronis	Basalt_5_15_1.8	1.66	167	S type	Convexity of largest fragments suggests more head-on than oblique impact.
	Basalt_3_15_1.4	1.69			
163 Erigone	Basalt_7_15_2.2	1.20	114	C/X type	
	Basalt_4_30_1.8	1.10			
	Basalt_7_30_2.2	1.12			
170 Maria	Basalt_5_45_1.4	2.17	192	S type	
	Basalt_3_45_1.0	1.67			
221 Eos	Basalt_6_30_1.8	3.76	381	K type	Interlopers. Asteroids 423 and 507 (object number 1 and 6) removed from the SFD for the fit.
	Basalt_6_45_1.4	3.86			
283 Emma	Basalt_4_15_2.2	1.90	185		(283) Emma itself is a binary; this simulation also produces a satellite around the largest remnant that matches well the size of the observed companion of (283) Emma.
	Basalt_3_30_1.8	1.80			
293 Brasilia	Basalt_5_30_1.8	1.10	110	C/X type	Interlopers. Asteroid 293 (object number 1) removed from the SFD for the fit.
363 Padua	Basalt_4_30_1.8	1.05	106	C/X type	
	Basalt_5_45_1.8	1.07			
	Basalt_5_15_2.2	1.07			

Table 1 (*continued*)

Family	Simulation	Shift factor[a]	Mean D_{PB} (km)	Spectral characteristics[b]	Notes
396 Aeolia	Basalt_5_60_1.4	0.38	39		
	Basalt_3_45_1.8	0.37			
	Basalt_6_45_2.2	0.41			
410 Chloris	Basalt_6_30_2.2	1.58	154	C type	Assuming that the largest member is an interloper. The morphology of this family's SFD strongly suggests that either of the first or second largest member is an interloper. Although both objects have taxonomies consistent with the taxonomy of the other members of the family (C type), many members of the background population around the family have the same taxonomy.
	Basalt_4_45_1.8	1.50			
	Basalt_6_30_2.2	1.63	165		Assuming that the second largest member is an interloper.
	Basalt_7_45_2.2	1.67			
490 Veritas	Basalt_7_60_1.0	1.69	177	C, P, and D type	
	Basalt_6_45_1.8	1.85			
569 Misa	Basalt_7_15_2.2	1.24	117	C type	
	Basalt_7_30_2.2	1.13			
	Basalt_4_30_1.8	1.14			
606 Brangane	Basalt_5_15_2.2	0.50	46	S type	
	Basalt_5_60_1.0	0.43			
668 Dora	Basalt_4_45_1.0	1.58	165	C type	
	Basalt_4_30_1.4	1.73			
808 Merxia	Basalt_6_30_1.8	1.18	121	S type	
	Basalt_6_45_1.4	1.24			
832 Karin	Basalt_7_15_2.2	0.65	63	S type	
	Basalt_7_30_2.2	0.63			
	Basalt_7_45_1.8	0.61			
845 Naema	Basalt_4_45_1.4	0.81	81	C type	
	Basalt_4_30_1.8	0.80			
	Basalt_6_15_2.2	0.83			
847 Agnia	Basalt_5_45_1.4	0.61	61	S type	Like Basalt_7_30_2.2 ($D_{PB} = 66$ km) but with a larger D_{LR}/D_{SLR} ratio.
1128 Astrid				C type	Unlike any of our runs (very shallow), but most like the most oblique runs at 75 deg.
1272 Gefion				S type	Interlopers. Asteroids 83 and 481 (object number 1 and 2) removed from the SFD for the fit. Not quite like any of the SFDs produced in our simulations, although the convex shape of the SFD for the smaller fragments suggests a low-speed impact by a large projectile at a low impact angle.
1639 Bower	Basalt_7_45_1.4				Interlopers. Asteroid 1639 (object number 1) removed from the SFD for the fit.
1644 Rafita	Basalt_6_45_1.8	0.63	63	S type	
1726 Hoffmeister	Basalt_7_45_1.4	1.50	134	C or F type	
	Basalt_3_15_1.4	1.18			
3556 Lixiaohua	Basalt_7_45_1.0	3.02	220	C/X type	
	Basalt_7_30_1.4	2.70			
	Basalt_4_45_1.0	1.54			
	Basalt_5_30_1.4	2.51			
	Basalt_4_15_1.4	1.87			
	Basalt_7_45_1.4	1.55			

[a] The factor in log(N) versus log(D) space required by which the modeled family must be 'slid' horizontally in order to produce a good fit to the observed family SFD.

[b] From Table 1 of Nesvorný et al. (2005) and Table 1 of Cellino et al. (2002).

logical match. Nevertheless, this criterion yields a parent body diameter of $D = 28$ km, comparable to the results of Nesvorný et al. (2006). This example illustrates the importance of using different fitting criteria when comparing SPH/N-body model results to data, particularly when the most diagnostic features of a family's SFD are unknown. For this reason, we are careful in Section 4.2 to compare our automated best-fit curve-matching results with those produced by more subjective 'eyeball' fits.

Similarly, in an ongoing study, we are using an artificial intelligence tool, sim_learn (Burl et al., 2006), to verify the accuracy of our scaled estimates for the (283) Emma family parent body size. The best match found so far by the intelligent tool is equivalent to a Basalt_4.6_55.4_1.38 simulation with a parent body diameter of 167 km. This result is relatively close to the two best scaled results reported here, but it is not an exact match. The target body diameter is smaller, and the impactor diameter, speed, and impact angle are all larger. The intelligent tool found other close matches at Basalt_3.8_50.5_0.89 with a 192-km-diameter target, Basalt_5.4_59.8_1.15 with a 175-km-diameter target, and Basalt_3.9_65.2_0.73 with a 164-km-diameter target. These results seem to push us toward a best-match region in our simulation matrix with smaller targets, larger impactors, and higher impact angles.

These examples from more detailed investigations via family-specific simulations suggest an uncertainty in our derived parent body diameters of a few tens of kilometers, inherent in the assumptions of the technique itself.

We suggest a further caution. C type and related taxonomic classes of asteroids are believed to contain a high degree of porosity (as indicated by their very low bulk densities) and processes such as pore crushing and compaction, not formally treated in our SPH3D simulations, probably play a significant role in cratering and disruption processes in these asteroids. While the solid basalt target asteroids used in our numerical simulations are probably valid comparisons to S-class and related taxonomic classes of asteroids, comparison of our model results with the properties of C type and related classes might be more problematic.

4.2. Using asteroid families as constraints for main-belt evolution models

A primary goal of this project has been to compile asteroid family data that can be used to constrain collision evolution models of the main belt as well as the poorly understood disruption scaling law governing asteroids and planetesimals. At present, the best available data on asteroid disruptions come from laboratory experiments, nuclear bomb blasts (e.g., Holsapple et al., 2002) and SPH models similar to those used here (e.g., Benz and Asphaug, 1999; Michel et al., 2001). While these lines of data provide useful insights, they also have considerable uncertainties. For example, most of the data on high energy explosions comes from underground nuclear bomb experiments that are orders of magnitude lower in energy than those needed to break apart multi-km asteroids. Asteroid families, however, provide a natural laboratory for these kinds of breakups, provided one can correctly interpret the data.

Our results suggest that previous studies (e.g., Tanga et al., 1999) may in some cases have significantly underestimated parent body sizes. We find that there are ∼20 families produced by catastrophic breakups in the main belt from parent bodies with diameters larger than 100 km, twice as many as previous estimates (Tanga et al., 1999). More specifically, if we break the main belt SFD into logarithmic size bins, with bin centers at $D = 123.5$, 155.5, 195.7, 246.4, 310.2, 390.5, and 491.6 km, the incremental number of families in each bin is 6, 5, 5, 1, 0, 1, and 1, respectively. Here we concentrated on large families because: (1) all such families are now believed to have been identified and (2) they cannot be ground away by collisions nor dispersed by Yarkovsky thermal drift forces on timescales short enough to make them disappear (Bottke et al., 2001, 2005a).

These values are comparable to those estimated by Bottke et al. (2005a, 2005b), who used a similar technique but subjective "eyeball" fits to estimate the incremental distribution of families (5, 5, 5, 1–2, 1, 1, 0) over the same size range. Given the fact that both the automated and subjective fit techniques have to account for the presence of interlopers, the unknown degree of collisional evolution within the largest families, and the marginal fit between some SPH runs and the existing families, it is encouraging that both yield family distributions similar to one another. It is also unclear which method provides a superior match to the family data; while there are certainly advantages in using automated fits that avoid human biases, much depends on how the "quality of fit" function was determined and how it was weighted on a per bin basis. We believe the best way to resolve this debate is not to modify our fitting technique but instead to improve our SPH model data using new runs specifically designed to simulate $D \gg 100$ km or $D \ll 100$ km family breakup events (e.g., Nesvorný et al., 2006). In particular, we will investigate the large Eos and Themis family-forming events that are responsible for the mismatch between Bottke et al. and this paper at the large end of the incremental distribution of families.

Before applying this family distribution to a main-belt evolution model, we need to know how long these families have been forming in the main belt. This is a tricky question to address because asteroid families are identified by their proper semi-major axes, eccentricities, and inclinations. Proper elements, which are quasi-integrals of motion, are computed by eliminating short and long-term perturbations from their osculating orbital elements (Knežević et al., 2002). To do this, we must assume that the planets providing the strongest perturbations have been in their current orbits over the interval of the calculation. We consider this a reasonable approximation for timescales of several billions of years.

If we go far enough back in time, however, it is unclear whether this assumption still holds. For example, recent numerical modeling work (Tsiganis et al., 2005; Morbidelli et al., 2005; Gomes et al., 2005) indicates the dynamical structure of the Solar System changed during the so-called Late Heavy Bombardment (LHB), a time period ∼3.8 Gyr ago when many of the largest basins on the Moon were formed (e.g., Tera et al., 1974; Stöffler and Ryder, 2001). According to this modeling work, the jovian planets were driven to their current a,

e, *i* orbital parameters during the LHB. In the process, secular resonances swept across the main belt and scattered ∼90% of the main-belt population onto planet-crossing orbits (Gomes et al., 2005; Strom et al., 2005). If this model is realistic, asteroid families existing prior to the LHB were dispersed and eliminated by sweeping resonances. Moreover, we cannot consider proper element calculations extending back to this epoch valid until new and more sophisticated formulations are created. Thus, even families unaffected by sweeping resonances would be undetectable beyond the LHB epoch. Accordingly, we assume here that no known family is older than 3.8 Gyr old. This limit agrees with preliminary estimates of family ages from dynamical models (David Vokrouhlický, personal communication).

Bottke et al. (2005a, 2005b) used these family distribution constraints to test different asteroid disruption scaling laws within a main-belt evolution model. Their best-fit results were found to be an excellent match to the scaling laws predicted by SPH asteroid breakup simulations (Benz and Asphaug, 1999). We believe this outcome provides a useful consistency check for the family distribution predictions made here.

In contrast, comparisons between our family distribution estimates and the results of other main-belt evolution models (e.g., Durda et al., 1998; Cheng, 2004; O'Brien and Greenberg, 2005) indicate these models produce considerably more families from $D > 100$ km parent bodies than permitted by observations. Bottke et al. (2005a, 2005b) argued that we are probably not missing many main-belt families in this size range from observational selection effects or dispersal via Yarkovsky thermal forces (Bottke et al., 2001). If true, why do these codes produce too many families? Bottke et al. (2005a) argued that to reproduce the shape of the current main-belt SFD, many of these codes treat asteroid disruption scaling laws as a free parameter. Accordingly, because their initial conditions are not well constrained, their best fit scaling laws are often discordant with SPH impact experiments. To correct this problem, we advocate that future collision modeling work be tested against the distributions of asteroid families like those described here.

4.3. Future work

It is likely that initial target and/or projectile spin could change the results presented here significantly (perhaps by mimicking a different impact angle). Leinhardt and Richardson (2000) investigated this effect and found that spin resulted in egg-shaped largest remnants and enhanced satellite production (although they did not quantify the latter in detail). Given what is known about current asteroid spin distributions, it is likely that this is an important effect that needs to be modeled in the future.

Additionally, we are in the process of rerunning the entire matrix of impact simulations with rubble-pile rather than solid targets. Collisional evolution models (e.g., Davis et al., 1985, 1989, 2002; Campo Bagatin et al., 2001) suggest that most asteroids have been substantially fractured or shattered and reassembled by impacts since their formation. Recent numerical results by Michel et al. (2004a) indicate that pre-shattered aster-

oids behave very differently in impact events than undamaged ones.

References

Asphaug, E., Melosh, H.J., 1993. The Stickney impact of Phobos: A dynamical model. Icarus 101, 144–164.

Asphaug, E., Ryan, E.V., Zuber, M.T., 2002. Asteroid interiors. In: Bottke, W.F., Cellino, A., Paolicchi, P., Binzel, R.P. (Eds.), Asteroids III. Univ. of Arizona Press, Tucson, pp. 463–484.

Benz, W., Asphaug, E., 1995. Simulations of brittle solids using smooth particle hydrodynamics. Comput. Phys. Commun. 87, 253–265.

Benz, W., Asphaug, E., 1999. Catastrophic disruptions revisited. Icarus 142, 5–20.

Bottke Jr., W.F., Durda, D.D., Nesvorný, D., Jedicke, R., Morbidelli, A., Vokrouhlický, D., Levison, H.F., 2005a. The fossilized size distribution of the main asteroid belt. Icarus 175, 111–140.

Bottke Jr., W.F., Durda, D.D., Nesvorný, D., Jedicke, R., Morbidelli, A., Vokrouhlický, D., Levison, H.F., 2005b. Linking the collisional history of the main asteroid belt to its dynamical excitation and depletion. Icarus 179, 63–94.

Bottke Jr., W.F., Durda, D., Nesvorný, D., Jedicke, R., Morbidelli, A., Vokrouhlický, D., Levison, H.F., 2005c. The origin and evolution of stony meteorites. In: Knežević, Z., Milani, A. (Eds.), Dynamics of Populations of Planetary Systems. IAU Colloquium 197, Belgrade. Cambridge Univ. Press, Cambridge, UK, pp. 357–376.

Bottke, W.F., Nolan, M.C., Greenberg, R., Kolvoord, R.A., 1994. Velocity distributions among colliding asteroids. Icarus 107, 255–268.

Bottke, W.F., Vokrouhlický, D., Brož, M., Nesvorný, D., Morbidelli, A., 2001. Dynamical spreading of asteroid families by the Yarkovsky effect. Science 294, 1693–1696.

Burl, M.C., DeCoste, D., Enke, B.L., Mazzoni, D., Merline, W.J., Scharenbroich, L., 2006. Automated knowledge discovery from simulators. In: Ghosh, J., Lambert, D., Skillicorn, D.B., Srivastava, J. (Eds.), Proceedings of the Sixth SIAM International Conference on Data Mining, April 20–22, 2006, Bethesda, MD, USA, SIAM, pp. 82–93, ISBN 0-89871-611-X.

Campo Bagatin, A., Petit, J.-M., Farinella, P., 2001. How many rubble piles are in the asteroid belt? Icarus 149, 198–209.

Cellino, A., Bus, S.J., Doressoundiram, A., Lazzaro, D., 2002. Spectroscopic properties of asteroid families. In: Bottke, W.F., Cellino, A., Paolicchi, P., Binzel, R.P. (Eds.), Asteroids III. Univ. of Arizona Press, Tucson, pp. 633–643.

Cheng, A.F., 2004. Collisional evolution of the asteroid belt. Icarus 169, 357–372.

Davis, D.R., Chapman, C.R., Weidenschilling, S.J., Greenberg, R., 1985. Collisional history of asteroids: Evidence from Vesta and the Hirayama families. Icarus 62, 30–53.

Davis, D.R., Weidenschilling, S.J., Farinella, P., Paolicchi, P., Binzel, R.P., 1989. Asteroid collisional evolution: Effects on sizes and spins. In: Binzel, R.P., Gehrels, T., Matthews, M.S. (Eds.), Asteroids II. Univ. of Arizona Press, Tucson, pp. 805–826.

Davis, D.R., Durda, D.D., Marzari, F., Campo Bagatin, A., Gil-Hutton, R., 2002. Collisional evolution of small-body populations. In: Bottke, W.F., Cellino, A., Paolicchi, P., Binzel, R.P. (Eds.), Asteroids III. Univ. of Arizona Press, Tucson, pp. 545–558.

Durda, D.D., Greenberg, R., Jedicke, R., 1998. Collisional models and scaling laws: A new interpretation of the shape of the main-belt asteroid size distribution. Icarus 135, 431–440.

Durda, D.D., Bottke, W.F., Enke, B.L., Asphaug, E., Richardson, D.C., Leinhardt, Z.M., 2003. The formation of asteroid satellites in catastrophic impacts: Results from numerical simulations. Lunar Planet. Sci. XXXIV. Abstract 1943.

Durda, D.D., Bottke, W.F., Enke, B.L., Merline, W.J., Asphaug, E., Richardson, D.C., Leinhardt, Z.M., 2004. The formation of asteroid satellites in large impacts: Results from numerical simulations. Icarus 170, 243–257.

Fujiwara, A., Cerroni, P., Davis, D., Ryan, E., Di Martino, M., Holsapple, K., Housen, K., 1989. Experiments and scaling laws for catastrophic collisions. In: Binzel, R.P., Gehrels, T., Matthews, M.S. (Eds.), Asteroids II. Univ. of Arizona Press, Tucson, pp. 240–265.

Gomes, R., Levison, H.F., Tsiganis, K., Morbidelli, A., 2005. Origin of the cataclysmic Late Heavy Bombardment period of the terrestrial planets. Nature 435, 466–469.

Holsapple, K., Giblin, I., Housen, K., Nakamura, A., Ryan, E., 2002. Asteroid impacts: Laboratory experiments and scaling laws. In: Bottke, W.F., Cellino, A., Paolicchi, P., Binzel, R.P. (Eds.), Asteroids III. Univ. of Arizona Press, Tucson, pp. 443–462.

Knežević, Z., Lemaître, A., Milani, A., 2002. The determination of asteroid proper elements. In: Bottke, W.F., Cellino, A., Paolicchi, P., Binzel, R.P. (Eds.), Asteroids III. Univ. of Arizona Press, Tucson, pp. 603–612.

Leinhardt, Z.M., Richardson, D.C., 2002. N-body simulations of planetesimal evolution: Effect of varying impactor mass ratio. Icarus 159, 306–313.

Leinhardt, Z.M., Richardson, D.C., Quinn, T., 2000. Direct N-body simulations of rubble pile collisions. Icarus 146, 133–151.

Michel, P., Benz, W., Tanga, P., Richardson, D.C., 2001. Collisions and gravitational reaccumulation: Forming asteroid families and satellites. Science 294, 1696–1700.

Michel, P., Benz, W., Tanga, P., Richardson, D.C., 2002. Formation of asteroid families by catastrophic disruption: Simulations with fragmentation and gravitational reaccumulation. Icarus 160, 10–23.

Michel, P., Benz, W., Richardson, D.C., 2003. Disruption of fragmented parent bodies as the origin of asteroid families. Nature 421, 608–611.

Michel, P., Benz, W., Richardson, D.C., 2004a. Catastrophic disruption of pre-shattered parent bodies. Icarus 168, 420–432.

Michel, P., Benz, W., Richardson, D.C., 2004b. Catastrophic disruption of asteroids and family formation: A review of numerical simulations including both fragmentation and gravitational reaccumulations. Planet. Space Sci. 52, 1109–1117.

Morbidelli, A., Nesvorný, D., Bottke, W.F., Michel, P., Vokrouhlický, D., Tanga, P., 2003. The shallow magnitude distribution of asteroid families. Icarus 162, 328–336.

Morbidelli, A., Levison, H.F., Tsiganis, K., Gomes, R., 2005. Chaotic capture of Jupiter's Trojan asteroids in the early Solar System. Nature 435, 462–465.

Nesvorný, D., Bottke, W.F., Levison, H.F., Dones, L., 2003. Recent origin of the Solar System dust bands. Astrophys. J. 591, 486–497.

Nesvorný, D., Jedicke, R., Whitely, R.J., Ivezić, Ž., 2005. Evidence for asteroid space weathering from the Sloan Digital Sky Survey. Icarus 173, 132–152.

Nesvorný, D., Enke, B.L., Bottke, W.F., Durda, D.D., Asphaug, E., Richardson, D.C., 2006. Karin cluster formation by asteroid impact. Icarus 183, 296–311.

O'Brien, D.P., Greenberg, R., 2005. The collisional and dynamical evolution of the main belt and NEA size distributions. Icarus 178, 179–212.

Richardson, D.C., Quinn, T., Stadel, J., Lake, G., 2000. Direct large-scale N-body simulations of planetesimal dynamics. Icarus 143, 45–59.

Ryan, E.V., 2000. Asteroid fragmentation and evolution of asteroids. Annu. Rev. Earth Planet. Sci. 28, 367–389.

Stadel, J., 2001. Cosmological N-body simulations and their analysis. Thesis. University of Washington, Seattle. 126 p.

Stöffler, D., Ryder, G., 2001. Stratigraphy and isotope ages of lunar geologic units: Chronological standard for the inner Solar System. Space Sci. Rev. 96, 9–54.

Strom, R.G., Malhotra, R., Ito, T., Yoshida, F., Kring, D.A., 2005. The origin of planetary impactors in the inner Solar System. Science 309, 1847–1850.

Tanga, P., Cellino, A., Michel, P., Zappalà, V., Paolicchi, P., Dell'Oro, A., 1999. On the size distribution of asteroid families: The role of geometry. Icarus 141, 65–78.

Tera, F., Papanastassiou, D.A., Wasserburg, G.J., 1974. Isotopic evidence for a terminal lunar cataclysm. Earth Planet. Sci. Lett. 22, 1–21.

Tillotson, J.H., 1962. Metallic equations of state for hypervelocity impact. General Atomic Report GA-3216.

Tsiganis, K., Gomes, R., Morbidelli, A., Levison, H.F., 2005. Origin of the orbital architecture of the giant planets of the Solar System. Nature 435, 459–461.

Zappalà, V., Cellino, A., 1996. Main belt asteroids: Present and future inventory. In: Rettig, T.W., Hahn, J.M. (Eds.), Completing the Inventory of the Solar System. In: Astronomical Society of the Pacific Conference Series, vol. 107. ASP, San Francisco, pp. 29–44.

Zappalà, V., Cellino, A., Dell'Oro, A., Paolicchi, P., 2002. Physical and dynamical properties of asteroid families. In: Bottke, W.F., Cellino, A., Paolicchi, P., Binzel, R.P. (Eds.), Asteroids III. Univ. of Arizona Press, Tucson, pp. 619–631.